Biomass Conversion

International Edition: DOI: 10.1002/anie.201603798
German Edition: DOI: 10.1002/ange.201603798

Simultaneous H_2 Generation and Biomass Upgrading in Water by an Efficient Noble-Metal-Free Bifunctional Electrocatalyst

*Bo You, Nan Jiang, Xuan Liu, and Yujie Sun**

Abstract: *As an environmentally friendly approach to generate H_2, electrocatalytic water splitting has attracted worldwide interest. However, its broad employment has been inhibited by costly catalysts and low energy conversion efficiency, mainly due to the sluggish anodic half reaction, the O_2 evolution reaction (OER), whose product O_2 is not of significant value. Herein, we report an efficient strategy to replace OER with a thermodynamically more favorable reaction, the oxidation of 5-hydroxymethylfurfural (HMF) to 2,5-furandicarboxylic acid (FDCA), catalyzed by 3D Ni_2P nanoparticle arrays on nickel foam (Ni_2P NPA/NF). HMF is one of the primary dehydration intermediates of raw biomass and FDCA is of many industrial applications. As a bifunctional electrocatalyst, Ni_2P NPA/NF is not only active for HMF oxidation but also competent for H_2 evolution. In fact, a two-electrode electrolyzer employing Ni_2P NPA/NF for simultaneous H_2 and FDCA production required a voltage at least 200 mV smaller compared with pure water splitting to achieve the same current density, as well as exhibiting robust stability and nearly unity Faradaic efficiencies.*

To address the challenges of impending global energy needs and associated climate change resulting from unsustainable fossil fuel consumption, great efforts have been devoted to exploiting clean and renewable alternative energy sources (such as solar and wind).[1] H_2, when generated from water splitting with renewable energy inputs, is a green energy carrier and is predicted to play a significant role in a future sustainable energy sector.[2,3] Unfortunately, the sluggish kinetics of the two half-reactions of water splitting, the H_2 and O_2 evolution reactions (HER and OER), require high overpotentials to achieve appreciable catalytic current density, resulting in relatively low energy conversion efficiencies.[4] At present, the prevailing approach to this challenge is the rational design and synthesis of highly active, stable, and cost-effective catalysts. For example, transition metal carbides,[5] nitrides,[6] phosphides,[7] sulfides,[8] and selenides[9] have been reported with promising HER catalytic performances. On the other hand, many transition metal oxides,[10] hydroxides,[11] and oxyhydroxides[12] exhibit attractive OER activities. More recently, nonprecious bifunctional catalysts with both HER and OER activities have also been reported.[13] In spite of these advances, OER is still the bottleneck of overall water splitting and demands a much higher overpotential to match the rate of HER.[5–13] In addition, the product of OER, O_2, is not of significant value and the potential mixing of H_2 and O_2 in the headspace of an electrolyzer poses safety concerns, requiring costly gas separation steps. Therefore, we reasoned that replacing OER with thermodynamically more favorable biomass oxidation reactions would not only generate value-added products at both electrodes (H_2 and updated bioproducts), but also increase the energy conversion efficiency of an electrolyzer.[14]

Biorefinery, referring to conversion of biomass into fuels and chemicals, is a complementary and attractive alternative to petroleum refining because biomass consists of contemporary carbon and its utilization will not alter our current ecosystem.[15] Among many biomass-derived intermediates, 5-hydroxymethylfrufural (HMF) has been classified as one of the top biomass-derived building block chemicals and can be used as a versatile precursor for the production of fine chemicals, plastics, pharmaceuticals, and liquid fuels.[16] For instance, one of its oxidation products, 2,5-furandicarboxylic acid (FDCA, Scheme 1), can serve as a monomer to produce

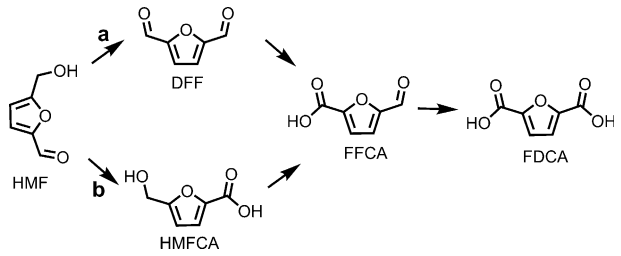

Scheme 1. Two possible pathways of HMF oxidation to FDCA.

polyamides, polyesters, and polyurethanes, being a replacement of terephthalic acid.[16] Although the conversion of HMF to FDCA has been reported, most previous catalytic systems were conducted under high-pressure O_2 or air at elevated temperatures and catalyzed by precious metals, such as Au, Pd, Pt, or their alloys.[15] In this regard, electrocatalytic oxidation offers an more sustainable strategy as the conversion will be driven by electricity and no chemical oxidants are necessary. Preferably, the electrocatalytic oxidation of HMF to FDCA will be solely catalyzed by low-cost catalysts and carried out under ambient conditions (1 atm and room temperature). However, very few electrocatalytic systems

[*] Dr. B. You, N. Jiang, X. Liu, Dr. Y. Sun
Department of Chemistry and Biochemistry
Utah State University
0300 Old Main Hill, Logan, UT 84322 (USA)
E-mail: yujie.sun@usu.edu
Homepage: http://www.yujiesun.org
Supporting information and the ORCID identification number(s) for the author(s) of this article can be found under http://dx.doi.org/10.1002/anie.201603798.

have been reported for HMF oxidation. The recent work of Choi et al. employed a redox mediator (TEMPO) to facilitate the HMF oxidation and expensive electrodes were utilized (Au and Pt), both of which resulted in high cost of the whole process.[17] We propose that it will be economically attractive if inexpensive catalysts could be developed to integrate both oxidative biomass valorization and H_2 generation under ambient conditions.

Herein, we report a bifunctional electrocatalyst of 3D Ni_2P nanoparticle arrays on nickel foam (Ni_2P NPA/NF) to couple HMF oxidation and H_2 evolution in alkaline media. Ni_2P NPA/NF was readily prepared by a scalable and lost-cost method, phosphidation of commercial nickel foam. Owing to the excellent catalytic performance of Ni_2P NPA/NF for HMF oxidation relative to OER, a two-electrode electrolyzer employing the Ni_2P NPA/NF catalyst couple on both cathode and anode was able to produce high current density (ca. 50 mA cm^{-2}) with a voltage at least 200 mV less than that of pure water splitting electrolysis. In addition, near unity Faradaic efficiencies were achieved for both H_2 (100%) and FDCA (98%) generation, together with robust stability. The low-cost composite and preparation method of Ni_2P NPA/NF, as well as its superior performance for H_2 and FDCA production, render the current catalytic systems very appealing for sustainable energy conversion technologies. It is also anticipated that this coupling concept can be extended to combine HER with many other oxidative biomass valorization reactions for diverse energy-related applications.

As a model electrocatalyst, the 3D bifunctional Ni_2P NPA/NF electrocatalyst was prepared by a facile and straightforward phosphidation of commercially available nickel foam (Supporting Information). The X-ray diffraction (XRD) pattern (Figure 1a) confirmed the partial transformation of metallic Ni to Ni_2P (PDF: 65-3544). Scanning electron microscopy (SEM) imaging (Figure 1b) indicated that Ni_2P NPA/NF still maintained the 3D macroporous framework of the pristine nickel foam (Figure S1a). While, the high-magnification SEM image of Ni_2P NPA/NF revealed its rough and porous morphology composed of numerous Ni_2P nanoparticles (Figure 1c), in sharp contrast to the smooth surface of the original nickel foam (Figure S1b). Figure 1d showed the corresponding elemental mapping images of Ni and P in Ni_2P NPA/NF, and demonstrated that both Ni and P were uniformly distributed throughout the whole sample, in agreement with the successful chemical conversion of metallic Ni to Ni_2P by the low-temperature phosphidation. X-ray photoelectron spectroscopy (XPS) analysis corroborated the presence of Ni and P in Ni_2P NPA/NF (Figure S2), in line with the elemental mapping results (Figure 1d). The high-resolution Ni $2p_{3/2}$ spectrum was fitted by three sub-peaks at binding energies of 853.1, 854.4, and 860.4 eV (Figure S2a), assignable to $Ni^{\delta+}$ in Ni_2P, oxidized Ni species, and the Ni $2p_{3/2}$ satellite peak of Ni_2P, respectively.[13g] Similarly, the high-resolution P 2p XPS spectrum (Figure S2b) could be deconvoluted into three sub-peaks at 129.3, 130.0, and 134.3 eV, corresponding to P $2p_{3/2}$, P $2p_{1/2}$, and oxidized P species (arising from superficial oxidation due to exposure in air), respectively.[7c–e] The Ni 2p peak at 853.1 eV was positively shifted compared to that of metallic Ni ($\approx$852.5 eV) and the P 2p peak at 129.3 eV

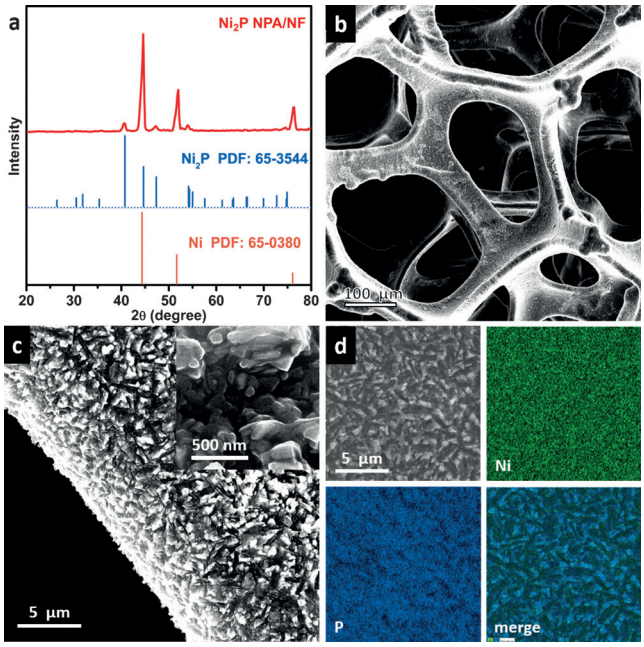

Figure 1. a) XRD pattern of Ni_2P NPA/NF with the corresponding standard patterns of Ni_2P and Ni. b,c) SEM images of Ni_2P NPA/NF at different magnifications. d) SEM and the corresponding elemental mapping images of Ni_2P NPA/NF.

was negatively shifted relative to that of elemental P (130.2 eV). These binding energy shifts imply that Ni in Ni_2P NPA/NF has a partial positive charge (δ^+) while P has a partial negative charge (δ^-), indicative of charge transfer from Ni to P, consistent with previous reports.[7c–e]

For the electrocatalytic oxidation of HMF in an aqueous electrolyte (1.0 M KOH), OER is the major competing reaction. Therefore, the electrochemical HMF oxidation and OER catalyzed by Ni_2P NPA/NF were first compared by linear sweep voltammetry (LSV; Figure 2a). In the absence of HMF, Ni_2P NPA/NF exhibited a catalytic onset potential of ~1.50 V vs. RHE (reversible hydrogen electrode) and high catalytic current density beyond 1.60 V vs. RHE, suggesting excellent OER activity. Upon the addition of 10 mM HMF, the onset potential shifted to 1.35 V vs. RHE, and a rapid current density rise could be observed within 1.40 V vs. RHE, indicating that the oxidation of HMF was significantly easier than OER catalyzed by Ni_2P NPA/NF. It is important to mention that the pristine nickel foam showed inferior performance for both OER and HMF oxidation (Figure S3), highlighting the important role of Ni_2P on nickel foam.

To identify and quantify the oxidation products as well as calculate the corresponding Faradaic efficiencies, Ni_2P NPA/NF-catalyzed HMF oxidation was performed by applying a constant potential of 1.423 V vs. RHE and passing charge of ~59 C (Figure S4). Based on our calculations, ~59 C corresponds to complete HMF oxidation to FDCA if a 100% Faradaic efficiency could be achieved. As shown in Figure 2a, no appreciable water oxidation could occur at 1.423 V, thus a high Faradaic efficiency for HMF oxidation was anticipated. High-performance liquid chromatography (HPLC) was used to monitor the concentration changes of HMF and its oxidation products during electrolysis (see the Supporting

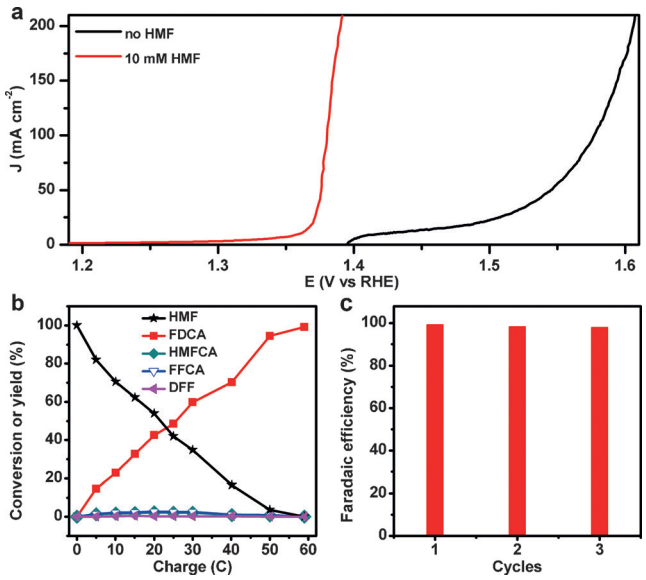

Figure 2. a) LSV curves of Ni_2P NPA/NF at a scan rate of 2 mV s^{-1} in 1.0 M KOH with and without 10 mM HMF. b) Conversion and yield (%) changes of HMF and its oxidation products during the electrochemical oxidation of HMF at 1.423 V vs. RHE in 1.0 M KOH with 10 mM HMF. c) Faradaic efficiencies of Ni_2P NPA/NF for FDCA production under three successive electrolysis cycles.

Information for details) and the resulting chromatograms (Figure S5) clearly showed the concentration decrease and rise of HMF and FDCA, respectively, over time, suggesting the conversion of HMF into FDCA (Figure 2b). After passing charge of ~59 C, the peak of HMF completely disappeared and the color of the electrolyte solution changed from pale yellow to colorless (Figure S5i, inset). The concentration changes of HMF, its oxidation intermediates, and FDCA during the electrolysis were plotted in Figure 2b, resulting in near unity Faradaic efficiencies for both HMF conversion and FDCA production.

Generally, there are two pathways for HMF oxidation: one is through an initial alcohol oxidation to form DFF as the intermediate (Scheme 1a), while the other is through an initial aldehyde oxidation to form HMFCA as the intermediate (Scheme 1b). Both pathways converge at the formation of FFCA prior to FDCA. In the present case, HMF oxidation catalyzed by Ni_2P NPA/NF likely followed the HMFCA route, as revealed by the relatively higher concentration of HMFCA compared to that of DFF (Figure 2b). This pathway is similar to other reported aerobic oxidation reactions.[18] However, the DFF route could not be completely excluded as DFF was also detected during electrolysis. The stability of Ni_2P NPA/NF for HMF oxidation was also investigated by performing three successive cycles of the constant potential electrolysis utilizing the same Ni_2P NPA/NF. As shown in Figure 2c, the calculated Faradaic efficiencies of FDCA formation for these electrolysis trials were in the range of 98–100%, illustrating the robust stability of Ni_2P NPA/NF for HMF oxidation.

Although the low-magnified SEM image (Figure S6a) and XRD pattern (Figure S7) of Ni_2P NPA/NF after HMF oxidation (named as post-HMF Ni_2P NPA/NF) indicated the inheritance of the overall 3D hierarchically porous configuration and primary Ni_2P phase, a close inspection of the post-HMF Ni_2P NPA/NF in the high-magnified SEM images (Figure S6b–d) revealed the presence of featureless monoliths and cracks, in contrast to the fresh sample (Figure 1c). Elemental mapping results (Figure S6d) demonstrated that the post-HMF Ni_2P NPA/NF mainly consisted of Ni and P, plus a large concentration of O over the newly formed monoliths. On the other hand, the high-resolution Ni $2P_{3/2}$ XPS spectrum of the post-HMF Ni_2P NPA/NF sample displayed an intensity decrease at 853.1 eV (assignable to Ni δ^+ in Ni_2P) while an increase at 856.9 eV (corresponding to oxidized Ni species), confirming the partial oxidation of Ni_2P (Figure S8a). This oxidation phenomenon was also revealed by the increased intensity of the peak ascribed to oxidized P species in the high-resolution P 2p XPS spectrum (Figure S8b). Taken together, it is safe to conclude that the real catalytically active sites for HMF oxidation reaction are the oxidized Ni species. These types of electrochemical oxidations have been commonly observed for many bifunctional water splitting electrocatalysts during OER.[13a,d–j]

To successfully couple HER and HMF oxidation for simultaneous H_2 and FDCA production, the Ni_2P NPA/NF electrocatalyst has to maintain excellent HER performance in the presence of HMF due to the potential permeation of HMF across the membrane from the anode compartment to the cathode site. Therefore, we sought to evaluate the impact of HMF on the HER activity of Ni_2P NPA/NF under the harshest condition (assuming all of the HMF was present in the cathode compartment). As demonstrated in Figure 3a,b, the HER LSV curves of Ni_2P NPA/NF in 1.0 M KOH before and after the addition of 10 mM HMF exhibited a small cathodic shift of 9 mV to reach −10 mA cm^{-2}, and the

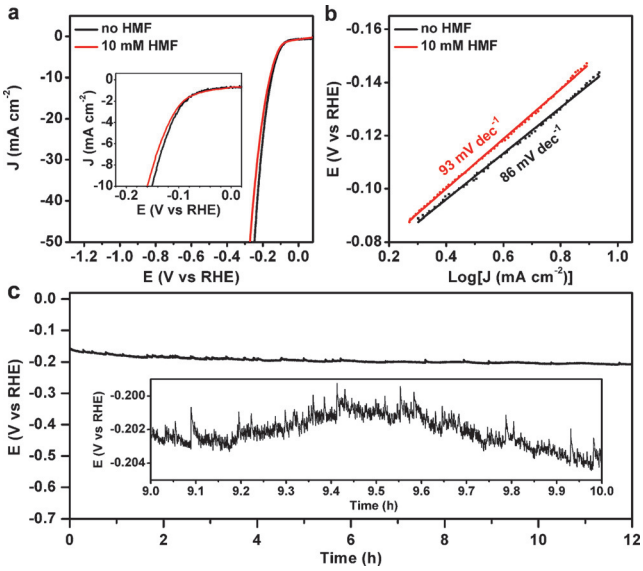

Figure 3. a) LSV curves and b) the corresponding Tafel plots of Ni_2P NPA/NF at a scan rate of 2 mV s^{-1} in 1.0 M KOH with and without 10 mM HMF. c) Chronopotentiometric curve of Ni_2P NPA/NF at −10 mA cm^{-2} in 1.0 M KOH containing 10 mM HMF. The inset in c) shows the expanded chronopotentiometric curve with oscillations due to the growth and release of H_2 bubbles on the catalyst surface.

calculated Tafel slope only increased from 86 to 93 mV dec^{-1} (Figure 3b). Additionally, a 12-h chronopotentiometry experiment conducted at a current density of −10 mA cm^{-2} in 1.0 M KOH containing 10 mM HMF demonstrated that the overpotential required to afford −10 mA cm^{-2} increased by less than 45 mV (Figure 3c). The fluctuationsin an expanded chronopotentiometric curve also implied the formation and release of H_2 bubbles on the catalyst surface (Figure 3c inset). Furthermore, XRD (Figure S7), XPS (Figure S8), and SEM (Figure S9) results of Ni_2P NPA/NF after the 12-h HER stability test in 1.0 M KOH with 10 mM HMF (named as post-HER with HMF Ni_2P NPA/NF) confirmed the retention of its morphology and composition. These results unambiguously demonstrated the negligible influence of HMF on the HER activity and the strong stability of Ni_2P NPA/NF under the current condition.

Given the excellent electrocatalytic HER and HMF oxidation performance of Ni_2P NPA/NF in the same electrolyte (1.0 M KOH with 10 mM HMF), we next assembled an electrolyzer in a two-electrode configuration using Ni_2P NPA/NF as both anode and cathode electrocatalysts to achieve simultaneous H_2 and FDCA generation. For comparison, overall water splitting was also tested for a Ni_2P NPA/NF catalyst couple in the absence of HMF. As shown in Figure 4a, the Ni_2P NPA/NF couple needed cell voltages of only 1.65 and 1.80 V to afford 10 and 50 mA cm^{-2}, respectively, lower than or comparable to those of recently reported nonprecious overall water splitting electrocatalysts, including Co-P (1.64 V for 10 mA cm^{-2}),[13a] NiFe LDH/NF (1.70 V for 10 mA cm^{-2}),[13b] Ni_3S_2/NF (1.76 V for 13 mA cm^{-2}),[13d] and Ni_5P_4/NF (1.70 V for 10 mA cm^{-2}),[13e] suggesting its exceptional performance for overall water splitting. Remarkably, after introducing 10 mM HMF, the cell voltages to reach 10 and 50 mA cm^{-2} were dramatically reduced to 1.44 and 1.58 V, respectively (Figure 4b), implying much better energy conversion efficiency of Ni_2P NPA/NF-catalyzed HER and HMF oxidation relative to water splitting alone.

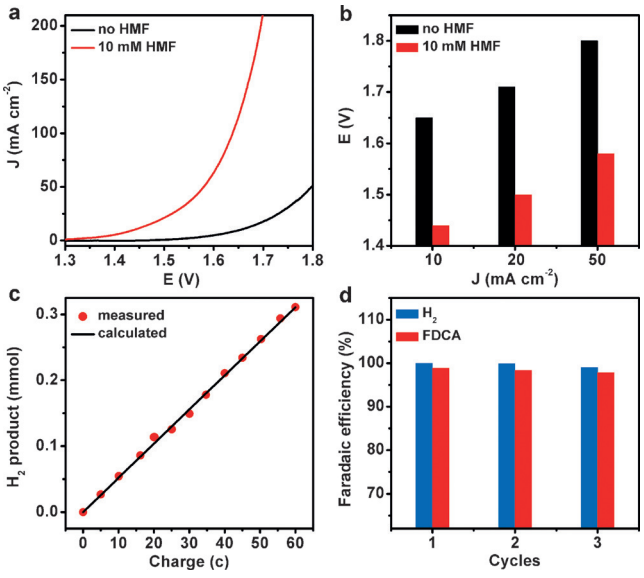

Figure 4. a) LSV curves and b) comparison of the overpotentials to achieve benchmark current densities (10, 20, and 50 mA cm^{-2}) for a Ni_2P NPA/NF catalyst couple in 1.0 M KOH with and without 10 mM HMF. c) GC-measured H_2 quantity compared with theoretically calculated H_2 quantity assuming a 100% Faradaic efficiency for the H_2 evolution catalysed by a Ni_2P NPA/NF catalyst couple in 1.0 M KOH solution with 10 mM HMF. d) Faradaic efficiencies of Ni_2P NPA/NF catalyst couple for simultaneous H_2 and FDCA generation in 1.0 M KOH solution with 10 mM HMF for three successive electrolysis cycles.

To quantify the produced H_2 and FDCA under a two-electrode configuration, a long-term electrolysis at a constant cell voltage of 1.50 V vs. RHE was performed to pass the charge of ~59 C. As shown in Figure 4c, the generated H_2 quantified by gas chromatography (GC) matched the calculated amount based on passed charge very well, leading to a Faradaic efficiency of 100%. Analysis of the resulting electrolyte by HPLC resulted in a ~98% Faradaic efficiency for FDCA production. It should be noted that such a long-term controlled potential electrolysis was repeated three times for the same Ni_2P NPA/NF catalyst couple and no apparent decrease in Faradaic efficiencies was observed (Figure 4d), supporting the outstanding stability of Ni_2P NPA/NF for integrated HER and HMF oxidation.

In summary, we have demonstrated a facile and efficient strategy for simultaneous H_2 production and biomass upgrading with Faradaic efficiencies of 100% and 98%, respectively, which was achieved using a bifunctional Ni_2P NPA/NF electrocatalyst. Owing to the more favorable thermodynamics and kinetics of HMF oxidation than OER catalyzed by Ni_2P NPA/NF, the cell voltage to reach benchmark current densities (10, 20, and 50 mA cm^{-2}) for H_2 production was significantly reduced by more than 200 mV, and concomitantly the oxidation product FDCA is much more valuable than raw HMF or O_2 from pure water splitting. Given the low cost for catalyst preparation, the high efficiency for the production of both H_2 and FDCA, as well as the abundance of substrates (H_2O and biomass), we envision that this strategy is very promising and practical for future energy conversion technologies. Moreover, this coupling concept is potentially extendable to combine HER with many other hydrocarbon oxidation reactions for various energy-related applications.

Acknowledgements

N.J. acknowledges the Governor's Energy Leadership Scholars Grant from the Utah Energy Research Triangle. This work was supported by Utah State University. We acknowledge the support of the Microscopy Core Facility at Utah State University for the SEM work. A provisional patent application by Y.S. has been filed for the intellectual property described in this communication. B.Y., N.J., and X.L. declare no competing financial interest.

Keywords: biomass upgrading · electrocatalysis · H_2 production · nickel phosphide

How to cite: *Angew. Chem. Int. Ed.* **2016**, *55*, 9913–9917
Angew. Chem. **2016**, *128*, 10067–10071

[1] a) S. Chu, A. Majumdar, *Nature* **2012**, *488*, 294 – 303; b) T. R. Cook, D. K. Dogutan, S. Y. Reece, Y. Surendranath, T. S. Teets, D. G. Nocera, *Chem. Rev.* **2010**, *110*, 6474 – 6502; c) V. S. Thoi, Y. Sun, J. R. Long, C. J. Chang, *Chem. Soc. Rev.* **2013**, *42*, 2388 – 2400.

[2] a) Y. Shi, B. Zhang, *Chem. Soc. Rev.* **2016**, *45*, 1529 – 1541; b) B. You, Y. Sun, *ChemPlusChem* **2016**, DOI: 10.1002/cplu.201600029; c) Y. Zheng, Y. Jiao, M. Jaroniec, S. Z. Qiao, *Angew. Chem. Int. Ed.* **2015**, *54*, 52 – 65; *Angew. Chem.* **2015**, *127*, 52 – 66; d) Y. Sun, J. Sun, J. R. Long, P. Yang, C. J. Chang, *Chem. Sci.* **2013**, *4*, 118 – 124; e) H. I. Karunadasa, E. Montalvo, Y. Sun, M. Majda, J. R. Long, C. J. Chang, *Science* **2012**, *335*, 698 – 702.

[3] a) E. M. Nichols, J. J. Gallagher, C. Liu, Y. Su, J. Resasco, Y. Yu, Y. Sun, P. Yang, M. C. Y. Chang, C. J. Chang, *Proc. Natl. Acad. Sci. USA* **2015**, *112*, 11461 – 11466; b) D. Kang, T. W. Kim, S. R. Kubota, A. C. Cardiel, H. G. Cha, K.-S. Choi, *Chem. Rev.* **2015**, *115*, 12839 – 12887; c) C. C. L. McCrory, S. Jung, I. M. Ferrer, S. M. Chatman, J. C. Peters, T. F. Jaramillo, *J. Am. Chem. Soc.* **2015**, *137*, 4347 – 4357.

[4] Y. Jiao, Y. Zheng, M. Jaroniec, S. Z. Qiao, *Chem. Soc. Rev.* **2015**, *44*, 2060 – 2086.

[5] a) R. Michalsky, Y. J. Zhang, A. A. Peterson, *ACS Catal.* **2014**, *4*, 1274 – 1278; b) C. Wan, Y. N. Regmi, B. M. Leonard, *Angew. Chem. Int. Ed.* **2014**, *53*, 6407 – 6410; *Angew. Chem.* **2014**, *126*, 6525 – 6528; c) H. B. Wu, B. Y. Xia, L. Yu, X. Y. Yu, X. W. Lou, *Nat. Commun.* **2015**, *6*, 6512; d) C. Wan, B. M. Leonard, *Chem. Mater.* **2015**, *27*, 4281 – 4288; e) R. Ma, Y. Zhou, Y. Chen, P. Li, Q. Liu, J. Wang, *Angew. Chem. Int. Ed.* **2015**, *54*, 14723 – 14727; *Angew. Chem.* **2015**, *127*, 14936 – 14940.

[6] a) W. F. Chen, K. Sasaki, C. Ma, A. I. Frenkel, N. Marinkovic, J. T. Muckerman, Y. Zhu, R. R. Adzic, *Angew. Chem. Int. Ed.* **2012**, *51*, 6131 – 6135; *Angew. Chem.* **2012**, *124*, 6235 – 6239; b) B. Cao, G. M. Veith, J. C. Neuefeind, R. R. Adzic, P. G. Khalifah, *J. Am. Chem. Soc.* **2013**, *135*, 19186 – 19192; c) W. F. Chen, J. T. Muckerman, E. Fujita, *Chem. Commun.* **2013**, *49*, 8896 – 8909.

[7] a) E. J. Popczun, J. R. McKone, C. G. Read, A. J. Biacchi, A. M. Wiltrout, N. S. Lewis, R. E. Schaak, *J. Am. Chem. Soc.* **2013**, *135*, 9267 – 9270; b) E. J. Popczun, C. G. Read, C. W. Roske, N. S. Lewis, R. E. Schaak, *Angew. Chem. Int. Ed.* **2014**, *53*, 5427 – 5430; *Angew. Chem.* **2014**, *126*, 5531 – 5534; c) P. Jiang, Q. Liu, Y. Liang, J. Q. Tian, A. M. Asiri, X. Sun, *Angew. Chem. Int. Ed.* **2014**, *53*, 12855 – 12859; *Angew. Chem.* **2014**, *126*, 13069 – 13073; d) Z. Xing, Q. Liu, A. M. Asiri, X. Sun, *Adv. Mater.* **2014**, *26*, 5702 – 5707; e) P. Xiao, W. Chen, X. Wang, *Adv. Energy Mater.* **2015**, *5*, 1500985; f) N. Jiang, B. You, M. Sheng, Y. Sun, *ChemCatChem* **2016**, *8*, 106 – 112.

[8] a) Y. Sun, C. Liu, D. C. Grauer, J. Yano, J. R. Long, P. Yang, C. J. Chang, *J. Am. Chem. Soc.* **2013**, *135*, 17699 – 17702; b) K. Chang, X. Hai, J. Ye, *Adv. Energy Mater.* **2016**, *6*, 1502555; c) D. Y. Wang, M. Gong, H. L. Chou, C. J. Pan, H. A. Chen, Y. Wu, M. C. Lin, M. Guan, J. Yang, C. W. Chen, Y. L. Wang, B. J. Hwang, C. C. Chen, H. Dai, *J. Am. Chem. Soc.* **2015**, *137*, 1587 – 1592; d) C. Di Giovanni, W. A. Wang, S. Nowak, J. M. Grenèche, H. Lecoq, L. Mouton, M. Giraud, C. Tard, *ACS Catal.* **2014**, *4*, 681 – 687; e) B. You, N. Jiang, M. Sheng, Y. Sun, *Chem. Commun.* **2015**, *51*, 4252 – 4255; f) N. Jiang, L. Bogoev, M. Popova, S. Gul, J. Yano, Y. Sun, *J. Mater. Chem. A* **2014**, *2*, 19407 – 19414; g) B. You, N. Jiang, Y. Sun, *Inorg. Chem. Front.* **2016**, *3*, 279 – 285; h) N. Jiang, Q. Tang, M. Sheng, B. You, D.-e. Jiang, Y. Sun, *Catal. Sci. Technol.* **2016**, *6*, 1077 – 1084.

[9] a) D. Kong, H. Wang, Z. Lu, Y. Cui, *J. Am. Chem. Soc.* **2014**, *136*, 4897 – 4900; b) H. Wang, D. Kong, P. Johanes, J. J. Cha, G. Zheng, K. Yan, N. Liu, Y. Cui, *Nano Lett.* **2013**, *13*, 3426 – 3433; c) Y. R. Zheng, M. R. Gao, Z. Y. Yu, Q. Gao, H. L. Gao, S. H. Yu, *Chem. Sci.* **2015**, *6*, 4594 – 4598.

[10] a) R. D. L. Smith, M. S. Prévot, R. D. Fagan, Z. Zhang, P. A. Sedach, M. K. J. Siu, S. Trudel, C. P. Berlinguette, *Science* **2013**, *340*, 60 – 63; b) J. Suntivich, K. J. May, H. A. Gasteiger, J. B. Goodenough, Y. Shao-Horn, *Science* **2011**, *334*, 1383 – 1385; c) T. Y. Ma, S. Dai, M. Jaroniec, S. Z. Qiao, *J. Am. Chem. Soc.* **2014**, *136*, 13925 – 13931.

[11] a) X. Lu, C. Zhao, *Nat. Commun.* **2015**, *6*, 6616; b) F. Song, X. Hu, *Nat. Commun.* **2014**, *5*, 4477.

[12] a) M. S. Burker, M. G. Kast, L. Trotochaud, A. M. Smith, S. W. Boettcher, *J. Am. Chem. Soc.* **2015**, *137*, 3638 – 3648; b) L. Trotochaud, S. L. Young, J. K. Ranney, S. W. Boettcher, *J. Am. Chem. Soc.* **2014**, *136*, 6744 – 6753; c) H. S. Ahn, A. J. Bard, *J. Am. Chem. Soc.* **2016**, *138*, 313 – 318.

[13] a) N. Jiang, B. You, M. Sheng, Y. Sun, *Angew. Chem. Int. Ed.* **2015**, *54*, 6251 – 6254; *Angew. Chem.* **2015**, *127*, 6349 – 6352; b) J. Luo, J.-H. Im, M. T. Mayer, M. Schreier, M. K. Nazeeruddin, N.-G. Park, S. D. Tilley, H. J. Fan, M. Grätzel, *Science* **2014**, *345*, 1593 – 1596; c) H. Jin, J. Wang, D. Su, Z. Wei, Z. Pang, Y. Wang, *J. Am. Chem. Soc.* **2015**, *137*, 2688 – 2694; d) L.-L. Feng, G. Yu, Y. Wu, G.-D. Li, H. Li, Y. Sun, T. Asefa, W. Chen, X. Zou, *J. Am. Chem. Soc.* **2015**, *137*, 14023 – 14026; e) M. Ledendecker, S. K. Calderón, C. Papp, H.-P. Steinrück, M. Antonietti, M. Shalom, *Angew. Chem. Int. Ed.* **2015**, *54*, 12361 – 12365; *Angew. Chem.* **2015**, *127*, 12538 – 12542; f) B. You, Y. Sun, *Adv. Energy Mater.* **2016**, *6*, 1502333; g) B. You, N. Jiang, M. Sheng, M. W. Bhushan, Y. Sun, *ACS Catal.* **2016**, *6*, 714 – 721; h) B. You, N. Jiang, M. Sheng, S. Gul, J. Yano, Y. Sun, *Chem. Mater.* **2015**, *27*, 7636 – 7642; i) Y. Yang, H. Fei, G. Ruan, J. M. Tour, *Adv. Mater.* **2015**, *27*, 3175 – 3180; j) L. A. Stern, L. Feng, F. Song, X. Hu, *Energy Environ. Sci.* **2015**, *8*, 2347 – 2351.

[14] Y. X. Chen, A. Lavacchi, H. A. Miller, M. Bevilacqua, J. Filippi, M. Innocenti, A. Marchionni, W. Oberhauser, L. Wang, F. Vizza, *Nat. Commun.* **2014**, *5*, 4036.

[15] Z. Zhang, K. Deng, *ACS Catal.* **2015**, *5*, 6529 – 6544.

[16] a) M. E. Zakrzewska, E. Bogel-Lukasik, R. Bogel-Lukasik, *Chem. Rev.* **2011**, *111*, 397 – 417; b) G. Lv, H. Wang, Y. Yang, T. Deng, C. Chen, Y. Zhu, X. Hou, *ACS Catal.* **2015**, *5*, 5636 – 5646.

[17] H. G. Cha, K.-S. Choi, *Nat. Chem.* **2015**, *7*, 328 – 333.

[18] S. E. Davis, B. N. Zope, R. J. Davis, *Green Chem.* **2012**, *14*, 143 – 147.

Received: April 19, 2016
Revised: June 20, 2016
Published online: July 15, 2016

